communications earth & environment

Article

A Nature Portfolio journal

https://doi.org/10.1038/s43247-025-02692-5

# Redox evolutions of planetary mantle reservoirs constrained by titanium isotopes



Zhengbin Deng [1,2,3] ✉, Katrine Nikolajsen[1], Martin Schiller [1], Lu Pan [1,3,4], Wenzhong Wang [4] & Martin Bizzarro [1]

The oxygen fugacity (hereafter referred as $fO_2$) of terrestrial planets is key in defining the outcome of planetary-scale differentiation and the planets' potential habitability. Reconstructing the initial $fO_2$ records in the mantle right after core formation for terrestrial planets remain challenging due to frequent secondary modifications. Here, we show based on studies of ureilites and diogenites that measurable Ti isotope fractionation occurred during melt extraction from planetary mantle in the presence of $Ti^{3+}$, and demonstrate that Ti isotopes can serve as a $fO_2$ tracer of planetary mantle reservoirs. We also show a positive correlation between the $^{49}Ti/^{47}Ti$ and La/Yb ratios for shergottites, which, when integrated with chronological constraints, imply the occurrence of Ti isotope fractionations arising from the presence of $Ti^{3+}$ during early mantle differentiation of Mars. Further constraints define reducing conditions of ~ΔIW–0.8 to ~ΔIW–1.6 for early-formed martian mantle reservoirs at ~4.5 Ga. This $fO_2$ estimate coincides with the lowest recommended values from martian meteorites, that of core-mantle differentiation for Mars and of diogenites, but is more oxidizing than that of ureilites. Mantle outgassing under these conditions would result in a reducing primordial atmosphere that is in stark contrast with Mars' current $CO_2$-dominated atmosphere.

Oxygen fugacity (hereafter referred to as $fO_2$) is a critical physico-chemical parameter that impacts the evolution and potential habitability of terrestrial planets. Initial $fO_2$ conditions of different planetary bodies are primarily controlled by the nature of the accreted materials (e.g., various groups of chondrites, bodies with more or less ice, and differentiated bodies, and so on), which can be further modified by processes such as mantle outgassing during the accretion and differentiation stage, and as well mantle equilibration with the nebular gas. Specifically, the initial $fO_2$ conditions of planetary mantle reservoirs following planet formation influence primary planetary-scale differentiation processes, including the degassing behavior of volatiles such as hydrogen, carbon, nitrogen, and oxygen[1–5] and the partitioning behavior of other elements between distinct chemical reservoirs during core-mantle and mantle-crust differentiation[6,7]. Thus, differences in initial $fO_2$ conditions have a profound impact not only on compositional evolution of a planet's oceans and atmospheres, but also on its thermal and geodynamical evolution[1–4,6,7].

Existing $fO_2$ estimates of planetary materials rely on petrological experiments and studies of phase equilibrium relations during magma crystallization such as mineral equilibrium assemblages[8,9], partitioning of redox-sensitive transition metals between minerals and melts[10–12], and the valence states of redox-sensitive transition metals in minerals[13,14]. Based on these approaches, a wide variability of $fO_2$ conditions in Solar System materials spanning ~14 orders of magnitude has been identified[14]. Despite this, there remain controversies on the $fO_2$ conditions of the mantle reservoirs right after core-mantle differentiation for terrestrial planets, in particular that for Mars[8–10,15–19]. This is because the primordial $fO_2$ conditions in the mantles of large rocky bodies are hard to determine, e.g., these records can be overprinted by later fluid/melt metasomatism in the mantle[20] or the $fO_2$ records of mantle-derived magmas can be readily modified by assimilation and degassing processes during magma ascent into the planetary crusts[18,21]. Thus, a full understanding of the initial $fO_2$ conditions of planetary mantle reservoirs requires a proxy that is insensitive to modification by secondary planetary and/or magmatic processes.

[1]Centre for Star and Planet Formation, Globe Institute, University of Copenhagen, Copenhagen, Denmark. [2]State Key Laboratory of Lithospheric and Environmental Coevolution, School of Earth and Space Sciences, University of Science and Technology of China, Hefei, 230026, China. [3]Deep Space Exploration Laboratory, Hefei, 230026, China. [4]Laboratory of Seismology and Physics of the Earth's Interior, School of Earth and Space Sciences, University of Science and Technology of China, Hefei, 230026, China. ✉e-mail: zhengbindeng@ustc.edu.cn

The stable isotope geochemistry of titanium is an emerging tool that can be used to determine the primary $fO_2$ conditions of planetary mantle reservoirs. Titanium has two valence states, namely $Ti^{3+}$ and $Ti^{4+}$, and below ΔIW + 0 (where ΔIW represents a difference of $fO_2$ of a system relative to the iron-wüstite buffer in a logarithmic unit), the proportion of $Ti^{3+}$ in basaltic silicate melts increases with progressively reducing conditions and approaches $Ti^{3+}/Ti^{4+} = 1$ at ~ΔIW−6.1[22]. In addition, first-principles calculations reveal that the presence of $Ti^{3+}$ can lead to Ti stable isotope fractionation of a sub per mil magnitude in $^{49}Ti/^{47}Ti$ ratio between pyroxene/pyrope and mafic silicate melts, with the $Ti^{3+}$ hosted by silicate minerals being enriched in the light Ti isotopes[23]. This is in contrast with $Ti^{4+}$, which exhibits insignificant isotope fractionation between silicate minerals and mafic silicate melts within an analytical uncertainty of ±0.015‰, as corroborated by studies of Earth's mantle and mantle-derived rocks[24–26], In a $Ti^{3+}$-bearing system, the extracted basaltic silicate melt from partial melting processes preferentially uptakes heavy Ti isotopes, leaving behind a residual mantle reservoir that is isotopically lighter. At the same degree of melt extraction, the magnitude of the light Ti isotope enrichment of the residual mantle may vary with $fO_2$, as prospected for the changing proportion of $Ti^{3+}$ in the melt. Compared to the $fO_2$ of the melt, the Ti stable isotopic composition of a magma is much less sensitive to modification by assimilation and degassing processes, offering an opportunity to determine via Ti isotopes the initial $fO_2$ conditions of planetary mantle reservoirs.

We recently developed protocols for ultra-high-precision Ti isotope measurements using a next-generation multi-collector inductively-coupled-plasma mass spectrometer (MC-ICP-MS), namely the *Neoma* MC-ICP-MS. This approach allows for the concomitant determination of the mass-dependent Ti isotope fractionation and nucleosynthetic variations in meteorites via a $^{47}Ti$-$^{49}Ti$ double-spike protocol[26]. The external reproducibility of the $\delta^{49}Ti$ (the per mil deviation in the $^{49}Ti/^{47}Ti$ ratio relative to OL-Ti standard) and $\varepsilon^{50}Ti$ (the per ten thousand deviation of the mass-bias-corrected $^{50}Ti/^{47}Ti$ ratio relative to the OL-Ti standard) values using our method are ±0.010‰ and ±0.15 epsilon, respectively[26]. This enables the identification of the probable minute Ti isotopic variability produced during magmatic processes in planetary mantle reservoirs, such as the mantle of the ureilite parent body, the Vesta mantle, and the martian mantle. Here, we intend to compare the Ti isotopic composition of meteorites with models of Ti isotope fractionation to quantify $fO_2$ conditions of the planetary mantles.

First, we focus on ureilites ($n = 9$) and diogenites ($n = 8$). Ureilites are understood to represent mantle residues of the ureilite parent body (UPB) after melt extraction at $fO_2$ conditions of ~ΔIW−3.3 to ~ΔIW−1.5[27,28]. It is noteworthy that melt extraction from UPB mantle has been dominated by graphite[29–31], leading to more reducing conditions relative to that of core formation for UPB set by high FeO contents of ureilites (~ΔIW−1) and thus plausibly larger Ti isotope fractionation due to the enhanced $Ti^{3+}/Ti^{4+}$ ratios in the melts during melt extraction in UPB mantle. Note that graphite metasomatism in ureilites after disruption of the UPB may further result in changes in olivine Mg# and impose at the microscale much more reducing conditions in ureilites[31]. However, this should have negligible effects on the Ti isotopic composition of ureilites on the whole-rock scale as the removal of silicate melts was supposedly very limited during this process. In contrast, diogenites are predominantly magma cumulates formed on the asteroid Vesta, and have slightly elevated $fO_2$ values of ~ΔIW−2 to ~ΔIW−0 relative to ureilites[14,32–34]. Both these types of achondrites represent products from melt-mineral segregation in the presence of $Ti^{3+}$ and, as such, are suited to evaluate the potential of Ti isotopes as a tracer for $fO_2$ during melt extraction in planetary mantle reservoirs and during subsequent magma differentiation.

Second, we apply Ti isotopes to constrain the initial $fO_2$ of the martian mantle. Previous studies of SNC meteorites have provided $fO_2$ estimates ranging from ~ΔIW−1 to ~ΔIW + 4[8–10,15–18]. Importantly, the $fO_2$ records of SNC meteorites broadly correlate with their geochemical features (e.g., La/Yb, $^{87}Sr/^{86}Sr$, and $^{143}Nd/^{144}Nd$ ratios), with the depleted samples being relatively reduced and the enriched ones more oxidized[8–10,17,18]. While it has been often inferred that the highly varying $fO_2$ values of SNC meteorites may represent the signals in the mantle sources[8,15–18], there remains a possibility that martian mantle may have a single, reducing $fO_2$ condition and the more oxidizing records are secondary during magma migration in the crust. As such, we have selected for study martian meteorites with various geochemical characteristics, i.e., 17 shergottites (four depleted, three intermediate, and ten enriched), one chassignite, and three nakhlites.

## Results

Our new measurements are reported in Fig. 1 together with previously published data for the same meteorite groups. Ureilites have low $\delta^{49}Ti$ values that vary from −0.105 ± 0.019‰ to −0.038 ± 0.019‰ compared to the chondrite average of +0.053 ± 0.005‰[26], except for EET 87517 that has a $\delta^{49}Ti$ value of +0.052 ± 0.004‰ (Fig. 1). We note that EET 87517 is also characterized by a higher $\varepsilon^{50}Ti$ value of −1.35 ± 0.03 relative to the other ureilites (−2.17 ± 0.24 to −1.63 ± 0.34) as well as a heavily oxidized interior such as the absence of iron metal and high $Fe^{3+}/(Fe^{2+} + Fe^{3+})$ ratio of 0.419[35]. Diogenites have $\delta^{49}Ti$ compositions that mostly cluster around or below the chondrite average, with Bilanga and NWA 4223 having the lowest $\delta^{49}Ti$ values of −0.039 ± 0.004‰ and −0.024 ± 0.007‰, respectively (Fig. 1).

Our new data for martian meteorites show a range of $\delta^{49}Ti$ values (−0.023 ± 0.007‰ to +0.138 ± 0.011‰), consistent within uncertainty with the earlier work[36] (Fig. 1). However, our high-precision data allows us to resolve a systematic difference in $\delta^{49}Ti$ between martian meteorite groups that correspond to geochemical enrichment, where the $\delta^{49}Ti$ values from depleted shergottites, intermediate shergottites, enriched shergottites to nakhlites/chassignite tend to increase and show larger inter-group variability (Fig. 1).

## Discussion

### Modeling Ti isotope fractionation during melt extraction in planetary mantle

Although there are a number of processes, in particular in magmatic systems on Earth, that can alter the Ti isotope composition of magmas and their residues, these mechanisms are not suited to account for the $\delta^{49}Ti$ variation in ureilites, diogenites, and shergottites. This is because on Earth, crystallization and separation of Ti-rich minerals (e.g., magnetite, ilmenite, and rutile) during processes such as fractional crystallization during magma migration and partial melting of crustal precursors are the major drivers of Ti isotope fractionation between magmatic rocks[24–26,37–40]. The formation of Fe-Ti oxides during magma differentiation, however, requires $fO_2$ conditions that exceed the typical range of $fO_2$ in ureilites, diogenites, and shergottites, and/or very evolved melt composition with MgO <5 wt%. While crystallization of armalcolite near the iron-wüstite buffer can also induce large Ti isotope fractionation[41], the saturation of armalcolite requires specific melt composition resembling that of high-Ti lunar mare basalts (i.e., $TiO_2$ contents over 10 wt%) that can be hardly approached in most ultramafic to mafic partial melts from other terrestrial planetary mantles.

Instead, for planetary objects like the parent bodies of ureilites and diogenites, and Mars, the relevant magmatic systems are dominated by ultramafic and mafic lavas, and felsic rocks such as those commonly present in Earth's continental crust are scarce or absent. Considering the negligible Ti isotopic fractionation of $Ti^{4+}$ between silicate minerals and mafic silicate melts based on Ti isotope data of Earth's igneous rocks[24–26] and by first-principles calculations[23], the $\delta^{49}Ti$ variations observed for ureilites and diogenites that have melting residue or cumulate origins require the presence of some amount of $Ti^{3+}$ in the magma systems. The magnitude of $Ti^{3+}$-induced Ti isotope fractionations during melt extraction from a planetary mantle can be modeled by combining: (i) the experimental calibration of $Ti^{3+}$ and $Ti^{4+}$ proportions in basaltic melts against $fO_2$[22] and (ii) the equilibrium Ti isotopic fractionation factors (i.e., $10^3 \ln\alpha$) of $Ti^{3+}$ and $Ti^{4+}$ in silicate minerals and basaltic melts that can be derived from first-principles calculations and studies of Earth's igneous rocks[23,24,26] (Fig. 2; see demonstration in Methods).

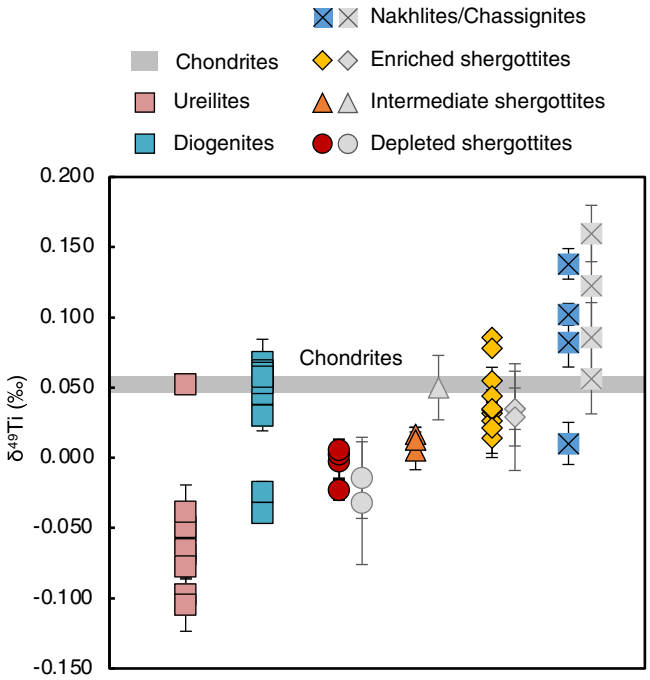


**Fig. 1 | Titanium isotopic results of ureilites, diogenites and martian meteorites.** Data of rock standards and meteorite samples from this study are provided in Tables S1, S2 in the Supplementary Materials. The chondrite average from ref. 26 and the literature data of martian meteorites from ref. 36 are shown in gray for comparison. Error bars represent the 2se uncertainties.

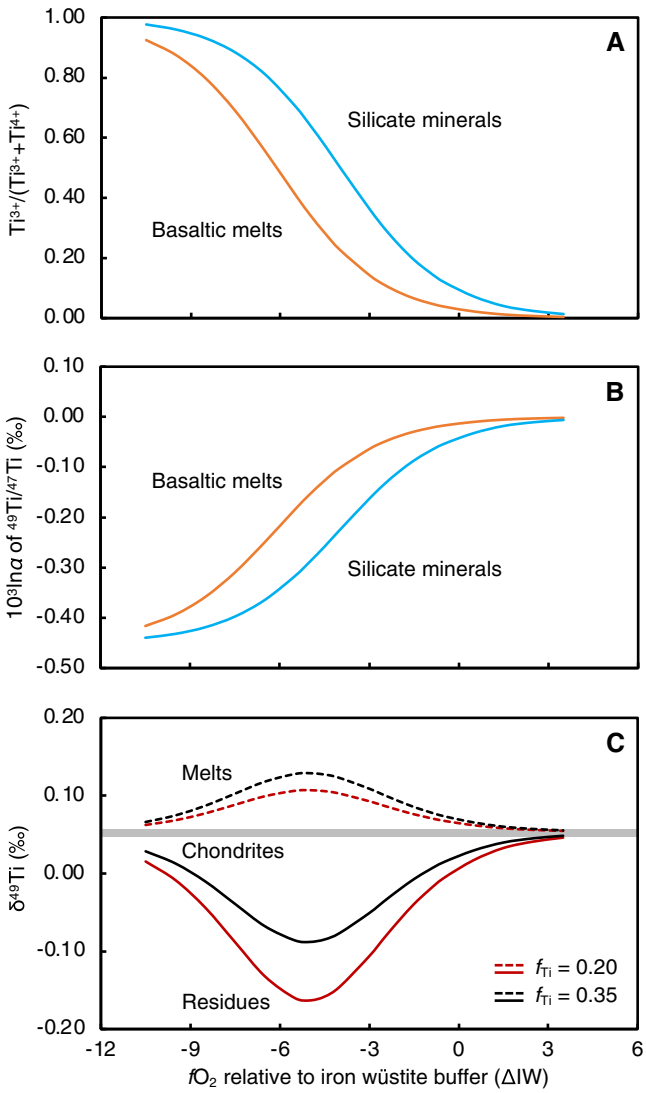


**Fig. 2 | Modeling Ti isotopic effects from $Ti^{3+}$ during melt extraction in planetary mantle. A** Valence states of Ti in basaltic melts and silicate minerals in equilibrium derived according to ref. 22. **B** Calculated equilibrium Ti isotope fractionation factors of basaltic melts and silicate minerals at varying $fO_2$ according to ref. 22–24,26. **C** Calculated Ti isotope fractionations in the extracted basaltic melts and melt-extracted residues in planetary mantle at varying $fO_2$ following two fractional melting scenarios (i.e., $f_{Ti} = 0.20$ and $f_{Ti} = 0.35$).

It is worth noting that in addition to $fO_2$, the $Ti^{3+}/(Ti^{4+}+Ti^{3+})$ ratio in the silicate melt in reality can be also a function of melt composition[22,42–44]. Therefore, some knowledge of the composition of the melt is needed before translating the $Ti^{3+}/(Ti^{4+}+Ti^{3+})$ ratio (and hence Ti isotopic variations) into $fO_2$. In this study, we adopt the calibration of the $Ti^{3+}/Ti^{4+}$ ratio against $fO_2$, i.e, $Ti^{3+}/(Ti^{4+}+Ti^{3+}) = 0.411$ at ~ΔIW–5.5, for the silicate melts at equilibrium with major mineral phases of planetary mantles (e.g., olivine, orthopyroxene, and clinopyroxene)[22], containing $SiO_2$ (47.52–54.79 wt%), $TiO_2$ (1.06–1.69 wt%), $Al_2O_3$ (10.03–21.12 wt%), FeO (0.19–0.65 wt%), MgO (15.08–15.73 wt%), and CaO (14.71–21.56 wt%). Notably, the melt products from the previously compiled calibration experiments[42] can contain $TiO_2$ contents over 25 wt%, which may have led to a non-ideal dependence of $Ti^{3+}/(Ti^{4+}+Ti^{3+})$ on $fO_2$[44]. Promisingly, consistent $Ti^{3+}/(Ti^{4+}+Ti^{3+})$-$fO_2$ relations, i.e., $Ti^{3+}/(Ti^{4+}+Ti^{3+}) = 0.359$–$0.426$ at ~ΔIW–5.5, have been obtained for the silicate melts at anorthite-diopside eutectic (or by addition of forsterite, enstatite, or wollastonite, i.e., $SiO_2 = 49.15$–$54.09$ wt%, $TiO_2 = 1.02$–$1.06$ wt%, $Al_2O_3 = 6.25$–$15.44$ wt%, MgO = 4.27–21.66 wt%, CaO = 14.31–37.43 wt%) in ref. 44 (Supplementary Fig. S1). A remaining caveat is that all the above-mentioned experimental melts[22,44] contain minor to no iron (FeO ≤0.65 wt%). Nonetheless, the consistency despite the wide chemical variability of the melt products for calibration[22,44] underscores the robustness of the used $Ti^{3+}/(Ti^{4+}+Ti^{3+})$-$fO_2$ calibration[22] to model melt depletion processes in terrestrial planetary mantles.

Due to the higher partition coefficients of $Ti^{3+}$ relative to $Ti^{4+}$ in silicate minerals (e.g., D $(Ti^{3+}) = 3.27 \times 10^{-1} \pm 2.58 \times 10^{-2}$ and D $(Ti^{4+}) = 9.54 \times 10^{-2} \pm 2.52 \times 10^{-3}$ for orthopyroxene; D $(Ti^{3+}) = 1.10 \times 10^{+0} \pm 7.82 \times 10^{-2}$ and D $(Ti^{4+}) = 2.87 \times 10^{-1} \pm 4.74 \times 10^{-3}$ for clinopyroxene)[22,43], at equilibrium the $Ti^{3+}/(Ti^{3+}+Ti^{4+})$ ratios in silicate minerals are higher than those in basaltic melts (Fig. 2A). Integrating with existing Ti isotope fractionation factors of $Ti^{3+}$ and $Ti^{4+}$ in silicate minerals and melts, basaltic melts have higher $10^3\ln\alpha$ (for the $^{49}Ti/^{47}Ti$ ratio) values than silicate minerals (Fig. 2B), meaning that extraction of basaltic melts from planetary mantle would preferentially uptake the heavier Ti isotopes and leave behind isotopically lighter melt-extracted residues. Furthermore, equilibrium Ti isotope fractionation factor between basaltic melts and melting residues, i.e., $10^3\ln\alpha$ (melt-residue), shows an inverted "U"-shaped dependence on $fO_2$, which increases from +0.004‰ at ~ΔIW + 3.5 to the maximum of +0.134‰ at ~ΔIW–5 and declines at $fO_2$ below ~ΔIW–5. As consequence, the Ti isotope fractionations in the extracted basaltic melts from fractional melting processes follow an inverted "U"-shaped dependence on $fO_2$, with the opposite recorded in the melt-extracted residues (Fig. 2C). This is because the maximum extent of isotope fractionation occurs while $Ti^{3+}/(Ti^{3+}+Ti^{4+})$ ratio approaches ~0.35 at ~ΔIW–5, where difference of the mean Ti valence between the melt and clino/orthopyroxene reaches maximal (i.e., 3.66 versus 3.36). It is worth noting that the magnitude of Ti isotope fractionation in the residual mantle would be larger at higher degrees of melt extraction, in other words, with lower Ti fraction ($f_{Ti}$) remaining in the melt-extracted residues (Fig. 2C).

## Stable Ti isotopic variation as a proxy for initial $fO_2$ conditions in planetary mantle reservoirs

The modeling results can be further compared to the $\delta^{49}Ti$ data of ureilites and diogenites for verification. For a chondritic precursor, a partial melting

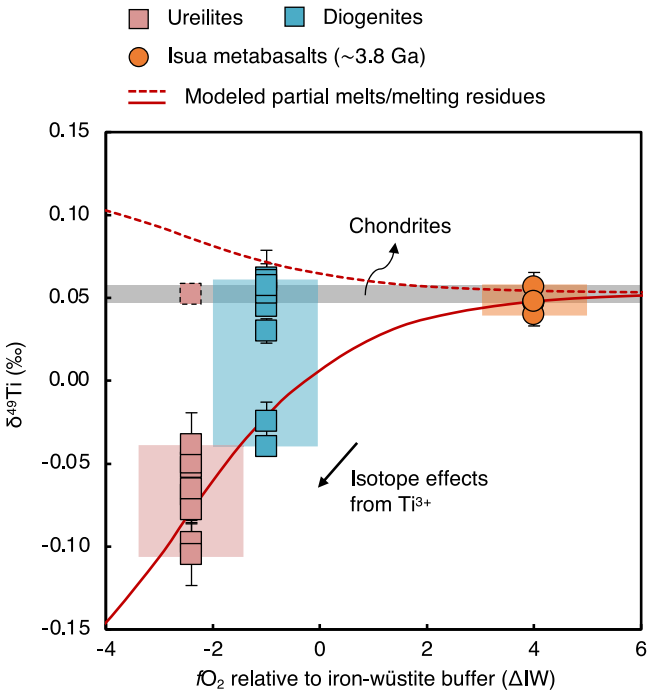


**Fig. 3 | Titanium isotopic effects from $Ti^{3+}$ as recorded by ureilites and diogenites.** The $\delta^{49}Ti$ data of the ~3.8 Ga Isua metabasalts are from ref. 26. Modeling results for melt extraction from a chondritic precursor with the presence of $Ti^{3+}$ are shown for comparison, where the red solid and red dashed curves represent partial melts and melting residues, respectively, after melt extraction at $f_{Ti} = 0.2$ (see Method for the modeling details). The shaded red, blue, and orange boxes cover the ranges of $\delta^{49}Ti$ and $fO_2$ for ureilites, diogenites, and Earth's upper mantle in the early Archean, respectively. Error bars represent the 2se uncertainties.

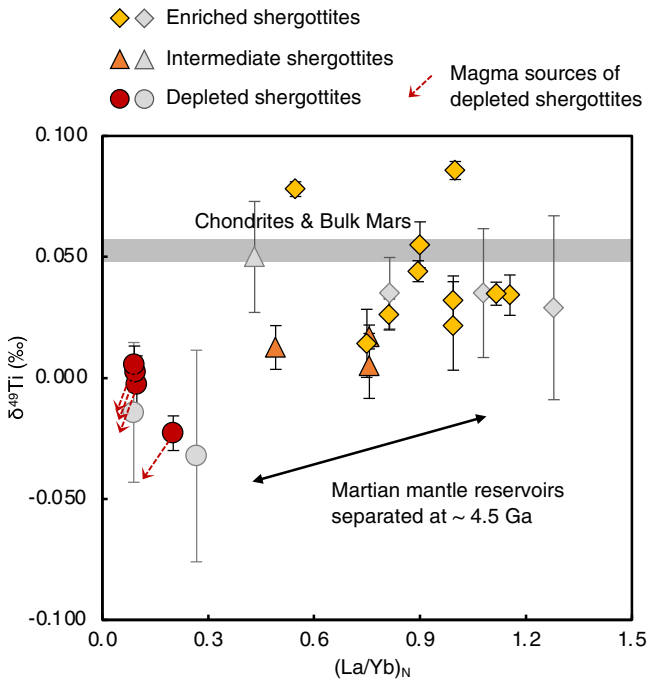


**Fig. 4 | Titanium isotope fractionation occurring during the ~4.5 Ga mantle differentiation event on Mars.** The chondrite average from ref. 26 and the literature data of martian meteorites from ref. 36 are shown in gray for comparison. The $(La/Yb)_N$ values of the martian meteorites have been calculated using the literature chemical data in the Martian Meteorite Compendium originally compiled by Charles Meyer and updated and revised by K. Righter in 2017, after a normalization onto the chemical data of chondrites in ref. 75. The red dashed arrows indicate the inferred $\delta^{49}Ti$ values of the magma sources for the depleted shergottites after correction of the Ti isotopic effects during magma generation as modeled in Fig. 2C. Error bars represent the 2se uncertainties.

event extracting ~80% Ti into a basaltic melt (i.e., $f_{Ti} = 0.20$, in other words a partial melting degree of ~20% at $D_{Ti} = 0.15$) via basaltic melt can produce isotope fractionations of up to ~0.22‰ in $\delta^{49}Ti$ for the residual mantle reservoir at the $fO_2$ conditions relevant to ureilites and diogenites (≤ΔIW + 0; Fig. 2C)[14], which can account for the lowest $\delta^{49}Ti$ values of ureilites (Fig. 3). With respect to diogenites that have cumulate origins, the same systematics may still hold, given that orthopyroxene and clinopyroxene from a reducing, $Ti^{3+}$-bearing basaltic melt should be enriched in $Ti^{3+}$ (and therefore the light Ti isotopes) relative to the melt (Fig. 3). Such Ti isotope fractionation between cumulates and melts may decrease or diminish in the case that the melts have become more oxidized (in other words containing much less or no $Ti^{3+}$ in the melts) due to degassing or wall-rock assimilation during magma migration. In this scenario, the cumulates would inherit the Ti isotopic composition of the silicate melts, which may be able to account for the elevated $\delta^{49}Ti$ values in most of the diogenite samples that plot above the modeled melting residue curve (Fig. 3). In comparison, the chondritic-like $\delta^{49}Ti$ value (+0.052 ± 0.004‰) for the anomalous ureilite (i.e., EET 87517) is in line with the highly oxidized nature of this sample, which most likely reflects admixing of oxidized carbonaceous chondrite materials to the ureilite parent body. This is further corroborated by the elevated $\varepsilon^{50}Ti$ value of this sample (−1.35 ± 0.03) relative to other ureilites (−2.17 to −1.63), as carbonaceous chondrites are characterized by the high $\varepsilon^{50}Ti$ values of +2 to +5[45]. The minimum $\delta^{49}Ti$ values defined by ureilites (i.e., −0.105 ± 0.019‰), diogenites (i.e., −0.039 ± 0.004‰), and the ~3.8 Ga Isua metabasalts broadly agree with the curve predicting isotopic effects from $Ti^{3+}$ during melt extraction in planetary mantle reservoirs (Fig. 3). Remarkably, the mean valences of Ti in the clinopyroxene and orthopyroxene from ureilite Y-791538 are 3.64 ± 0.05 and 3.68 ± 0.05, respectively[46]. Such redox states of Ti can be translated into $Ti^{3+}/(Ti^{3+} + Ti^{4+})$ ratios of 0.32-0.36 that are well consistent with the predicted $Ti^{3+}/(Ti^{3+} + Ti^{4+})$ ratios in clinopyroxene and orthopyroxene at ~ΔIW−3.0 to ~ΔIW−2.5 by the model in this study (0.30–0.36), representing independent evidence for $Ti^{3+}$ in ureilites. This establishes that Ti isotopes can serve as a sensitive tracer for $fO_2$ conditions during planetary mantle-crust differentiation.

## The primary redox state of the martian mantle constrained by Ti isotopes

Abundant chemical and Sr-Nd-Hf isotope systematics of martian meteorites suggest the existence of multiple chemical reservoirs in the martian mantle, which are usually referred to as depleted, intermediate, and enriched mantle sources of Mars[8,47–51]. The Sm-Nd model ages further imply that these mantle reservoirs have been separated from each other during a mantle differentiation event that can be dated back to as early as 4504 ± 6 Ma[52]. The $\delta^{49}Ti$ values of shergottites are positively correlated with the $(La/Yb)_N$ values (where "N" denotes a normalization to the same ratio in CI-type chondrites). Thus, similar to the trend observed for ureilites and diogenites, resolvable Ti isotope fractionations arising from $Ti^{3+}$ appear to have occurred during the ~4.5 Ga mantle differentiation event on Mars (Fig. 4). Based on the simulation of Ti isotopic effects from $Ti^{3+}$ (Fig. 2C), the lowest $\delta^{49}Ti$ value of −0.023 ± 0.007‰ for depleted shergottite Dhofar 019 corresponds to a $fO_2$ condition of ΔIW−1.0 ± 0.2 at the use of model of Ti isotope fractionation at $f_{Ti} = 0.2$ (Fig. 4). It is worth noting that the estimated $fO_2$ condition would be more reducing (i.e., ΔIW−1.4 ± 0.2) if adopting a larger $f_{Ti}$ value of 0.25 for the melt extraction model, in other words lower degree of Ti extraction from the mantle source. Nonetheless, depleted shergottites represent partial melts and their mantle sources are predicted to be characterized by even lower $\delta^{49}Ti$ values after taking into account the Ti isotopic effects from magma generation, e.g., $\Delta^{49}Ti_{\text{partial melt–source}}$ of +0.020‰ under an $fO_2$ condition close to ΔIW−1 at $f_{Ti} = 0.2$ (Fig. 4). This implies more reducing conditions (≤ΔIW−1) during the ~4.5 Ga mantle differentiation event on Mars.

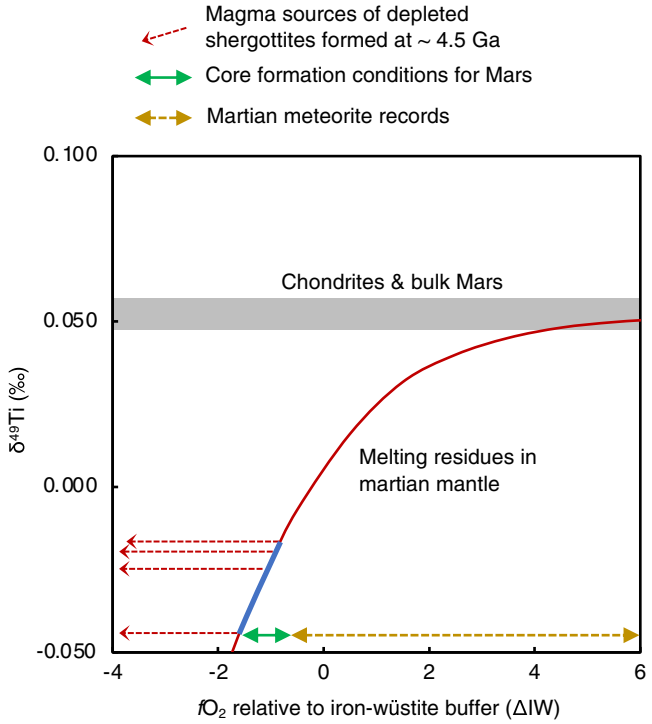


**Fig. 5 | Redox evolutions of Mars constrained by Ti isotopic results from this study.** The previously recommended $fO_2$ values of core formation for Mars[53,76] and martian meteorites[8–10,16–18] are shown for comparison. Modeling results for the melting residues in martian mantle, after melt extraction at $f_{Ti} = 0.20$ and varying $fO_2$ conditions in the presence of $Ti^{3+}$, are shown as a red solid curve (see Methods for the modeling details). The red dashed arrows indicate the inferred $\delta^{49}Ti$ values of the magma sources for the depleted shergottites after correction of the Ti isotopic effects during magma generation as modeled in Fig. 2C, which further define the blue section of the red model curve for melting residues in the martian mantle, translating into $fO_2$ conditions of ~ΔIW−1.6 to ~ΔIW−0.8 during prior melt depletion.

After correction of Ti isotopic effects from magma generation with a $\Delta^{49}Ti_{partial\ melt-source}$ value of +0.020‰, mantle sources of the four depleted shergottites in this study (i.e., NWA 4527, SaU 005, DaG 735, and Dhofar 019) have $\delta^{49}Ti$ values ranging from −0.043‰ to −0.014‰, which based on the previous simulation defines a $fO_2$ condition of ~ΔIW−1.6 to ~ΔIW−0.8 during the formation of the depleted mantle source of Mars at ~4.5 Ga (Fig. 5). This $fO_2$ range is in line with the core formation conditions (~ΔIW−1.25) of Mars inferred from Ni, Co, Mo, W, and P abundances in the martian mantle[53] or that (~ΔIW−1.7) inferred based on the FeO content of the martian mantle[54]. Importantly, the newly defined $fO_2$ condition of ~ΔIW−1.6 to ~ΔIW−0.8 for the ~4.5 Ga martian mantle also agrees with the lowest $fO_2$ values (~ΔIW−1) ever reported for martian meteorites, which have crystallization ages typically younger than ~1.4 Ga (Fig. 5)[8–10,16–19]. This consistency implies that the reducing mantle (≤ ΔIW−1) formed from the early differentiation of the martian mantle likely resided for an extended time period in the deep martian interior. Considering that the ancient martian crust has been greatly oxidized (up to ΔFMQ + 4) during impact-induced remelting at ~4.3-4.4 Ga[36,55,56], the predominantly oxidized nature of most previously studied shergottites and nakhlites[8–10,16–18] is likely secondary, reflecting admixing of crustal materials into their shallow mantle sources via impacts[36,57] or, alternatively, into evolving magmas by assimilation during migration and ascent in the crust[8,16].

### Implications for the evolution and potential habitability of Mars

The primary $fO_2$ condition of the martian mantle at ~4.5 Ga as constrained by Ti isotopes (i.e., ~ΔIW−1.6 to ~ΔIW−0.8) contrasts with that of Earth's upper mantle, which has been shown to be oxidized (i.e., ~ΔFMQ + 0) since 4.3–4.4 Ga[58,59]. It has been posited that Earth's upper mantle may have been oxidized to its modern state during and/or just after magma ocean solidification[4,60,61]. A deep magma ocean develops a vertical gradient in $fO_2$ at constant $Fe^{3+}/Fe^{2+}$ ratio and, as a result, the surface conditions can be up to 4–5 orders of magnitude more oxidizing than at the base of the terrestrial magma ocean[4,62,63]. Another related mechanism to enhance $fO_2$ in the upper mantle is iron disproportionation reaction in the solid state, arising from the preference of $Fe^{3+}$ over $Fe^{2+}$ for bridgmanite, which operates after core-mantle differentiation[60,61]. The reducing conditions of the martian mantle at ~4.5 Ga, as implied by $\delta^{49}Ti$ results of shergottites in this study, is consistent with those inferred from core-mantle differentiation, excluding noticeable iron disproportionation in the martian mantle.

Based on recent planetary outgassing models[2], the Earth's primordial atmosphere would be predominantly composed of $CO_2$ and $N_2$ after water condenses. The implied early martian mantle $fO_2$ conditions from our data, on the other hand, suggest that as early as ~4.5 Ga, Mars' atmosphere from mantle outgassing would have higher $H_2/H_2O$ and $CO/CO_2$ ratios at a given temperature. Such an early reducing atmosphere stands in contrast to the oxidizing state of the modern $CO_2$-dominated martian atmosphere[64,65], meaning that Mars may have gone through a transition in atmospheric composition in its geological history. Such a transition can occur at the cooling of an isochemical atmosphere[2], and/or may also relate to the delivery of water-rich asteroidal objects that induced impact remelting and subsequent oxidation of the ancient crust of Mars[36,57] and/or atmospheric hydrogen escaping through time[57]. Early martian crustal water reservoirs acquired a high D/H ratio of ~2–4 before ~4.1 Ga, possibly corresponding to this oxidation process, whereas later changes in D/H ratio might be due to secular hydrogen escape over the following 4 billion years[66].

Overall, our new results here suggest that Mars likely has time periods of a few hundred million years with reducing atmospheres, which can facilitate prebiotic chemistry forming complex organic molecules relevant for early life[67,68]. The shift in composition of the Martian atmosphere may have contributed to transitional phases in which increased $CO_2$-$H_2$ collision-induced absorption may sufficiently elevate the greenhouse effect to support liquid water on the surface of Mars ~3.7 billion years ago[57,69,70]. Such transition seems to be coeval with the oxidation of the ancient martian crust, which was later sampled by parent magmas of SNC meteorites[8–10,15–18]. Early reducing atmospheric conditions would more easily facilitate habitable conditions of Mars with a mild climate and available liquid water. Future missions that obtain samples containing the earliest geologic records during the transition of atmospheric/crustal oxidation state on Mars would advance our understanding of the origin of life during the geological evolution of terrestrial planets like Earth and Mars.

## Materials and methods

### Samples

The samples analyzed in this study include nine ureilites (i.e., DaG 319, GRO 95575, ALH 78019, ALH 84136, EET 87517, LEW 85328, MET 78008, PCA 82506, and EET 96042), eight diogenites (i.e., MET 00436, NWA 1461, NWA 4215, NWA 4223, NWA 5480, NWA 1821, Tatahouine, and Bilanga), and a set of martian meteorites that comprise four depleted shergottites (i.e., NWA 4527, SaU 005, DaG 735, and Dhofar 019), three intermediate shergottites (i.e., NWA 5029, NWA 480, and NWA 1950), ten enriched shergottites (i.e., JaH 479, NWA 2975, NWA 7258, NWA 7320, Shergotty, NWA 2990, NWA 4468, NWA 856, NWA 1068, and NWA 6963), one chassignite (i.e., NWA 2737), and three nakhlites (i.e., NWA 5790, NWA 817, and NWA 998).

### Sample dissolution and chromatographic purification of Ti

Powders of meteorite samples (~100 mg for each) or reference materials (i.e., AGV-2, BHVO-2, BCR-2, and BIR-1) were weighed into Savillex beakers and digested using mixtures of 22 M HF and 14 M $HNO_3$ acids with a volume ratio of 2:1 at 120 °C for 4 days. The samples were evaporated to dryness and re-dissolved in ~5–10 ml 6 M HCl at 120 °C. This process was repeated several times to decompose fluorides formed from HF dissolution until clear solutions were achieved. Afterwards, sample aliquots containing

~6 μg Ti were taken and properly mixed with a prepared $^{47}$Ti-$^{49}$Ti double spike, where Ti concentrations of sample solutions were determined in advance via a pre-spiked protocol to ensure consistent sample-spike mixing ratio between samples and standards[26]. The spiked sample aliquots were evaporated to dryness and re-dissolved in 6 M HCl overnight to achieve sample-spike equilibration. Titanium purification was carried out following a three-step protocol using AG1x8 (200–400 meshes) and DGA resins[26], which was modified after the earlier methods[25,71]. To remove potential trace amounts of Ca and Cr, the spiked OL-Ti standards and the final Ti cuts of meteorites and reference materials have been passed once more through the DGA columns before treatment in 14 M $HNO_3$ at 120 °C for destruction of the resin particles and organics inherited from column chemistry and final storage in 0.5 M $HNO_3$ + 0.01 M HF acids.

### Neoma MC-ICP-MS

Titanium isotopic compositions of the samples after purification were measured via the Thermo Fisher Scientific Neoma MC-ICP-MS, following an established sample introduction protocol[26]. An actively cooled membrane desolvation component with an APEX HF desolvating nebulizer from Elemental Scientific was used to stabilize the signals, and a sapphire injector was adopted to suppress oxide and silicon fluoride formation. In addition, $N_2$ gas at a rate of a few mL/min was added to enhance the sensitivity. Such instrumental settings return an intensity of ~15 V on $^{48}Ti^+$ for a solution of ~600 ppb Ti at an uptake rate of ~50 μL/min using medium mass resolution mode. The newly designed Neoma MC-ICP-MS has an increased mass dispersion (~20%) comparing to the earlier generation of instruments (~14%), which allows monitoring simultaneously ion species ranging from $^{43}Ca^+$ to $^{53}Cr^+$ in a single cup configuration[26] and thus avoids the use of a dynamic mode for data acquisition. Titanium isotopic data of the samples were measured following the previously described mass spectrometry settings and data acquisition strategies[26]. Importantly, monitoring signal intensities of $^{44}Ca^+$, $^{51}V^+$, and $^{53}Cr^+$ simultaneously with $^{46}Ti^+$, $^{47}Ti^+$, $^{48}Ti^+$, $^{49}Ti^+$, and $^{50}Ti^+$ permits a high-precision correction of isobaric interferences, after which a concomitant and high-precision derivation of $\delta^{49}$Ti and $\varepsilon^{50}$Ti values of samples can be achieved from the double-spike measurements[26]. As demonstrated by repeated experiments on chondrites (i.e., NWA 5697, NWA 530, NWA 1232, NWA 4428, and NWA 1563) and reference materials (i.e., BHVO-2, BCR-2, and AGV-2), the method provides long-term external reproducibilities of ± 0.010‰ and ± 0.15 epsilon for $\delta^{49}$Ti and $\varepsilon^{50}$Ti, respectively[26].

### Modeling of Ti isotopic effects from $Ti^{3+}$ during partial melting of a chondritic precursor

I. Quantifying proportions of $Ti^{3+}$ and $Ti^{4+}$ in silicate melts and minerals at varying $fO_2$

As earlier parameterized[22,43], redox reaction of Ti in silicate melts follows:

$$Ti^{3+}O_{1.5}(melt) + \frac{1}{4}O_2 = Ti^{4+}O_2(melt) \quad (1)$$

Petrological experiments in ref. 22 provide an empirical calibration of $Ti^{3+}$ and $Ti^{4+}$ proportions in basaltic silicate melts against $fO_2$ (Fig. 2A):

$$K'_{\mathrm{hom}} = \frac{[TiO_2(melt)]}{[TiO_{1.5}(melt)]} \times (fO_2)^{-\frac{1}{4}} \quad (2)$$

$$(K'_{\mathrm{hom}})^{-1} = 1.24 \times 10^{-4} \pm 1.31 \times 10^{-5} \quad (3)$$

This calibration was established for the silicate melts of basaltic to andesitic compositions, i.e., $SiO_2$ = 47.52–54.79 wt%, $TiO_2$ = 1.06−1.69 wt%, $Al_2O_3$ = 10.03–21.12 wt%, FeO = 0.19–0.65 wt%, MgO = 15.08–15.73 wt%, and CaO = 14.71–21.56 wt%[22]. This allows the derivation of the $Ti^{3+}$ proportion in a basaltic silicate melt at a chosen $fO_2$. While partitioning coefficients of $Ti^{3+}$ and $Ti^{4+}$ between minerals (e.g., orthopyroxene) and basaltic silicate melts have been experimentally determined, e.g., $D^{Ti^{3+}}(opx - melt) = 0.327$ and $D^{Ti^{4+}}(\mathrm{opx} - \mathrm{melt}) = 0.0954$[22], $Ti^{3+}$ and $Ti^{4+}$ proportions in orthopyroxene at equilibrium with basaltic silicate melts can be estimated via:

$$X^{Ti^{3+}}(opx) = \frac{X^{Ti^{3+}}(melt) \times D^{Ti^{3+}}(opx - melt)}{\left[1 - X^{Ti^{3+}}(melt)\right] \times D^{Ti^{4+}}(opx - melt) + X^{Ti^{3+}}(melt) \times D^{Ti^{3+}}(opx - melt)} \quad (4)$$

II. Modeling of Ti isotopic effects from $Ti^{3+}$ during melt extraction

In order to quantify the Ti isotopic effects during melt extraction in the presence of $Ti^{3+}$, it requires the Ti isotope fractionation factors between silicate minerals and silicate melts to be calibrated either by analyses of natural and experimental samples or by first-principles calculations. Here, we integrate existing constraints from literature:

i) First-principles calculations show that there can be some Ti isotope fractionations between $Ti^{4+}$-dominated orthopyroxene/clinopyroxene and $Ti^{3+}$-dominated orthopyroxene/clinopyroxene[23]. The equilibrium Ti isotope fractionation factor (i.e., $10^3 ln\alpha$ of $^{49}$Ti/$^{47}$Ti) of a phase can be formalized as:

$$10^3 ln\alpha = ax + bx^2 + cx^3 \quad (5)$$

where $x = 10^6/T^2$ with T as temperature in Kelvin.

For $Ti^{3+}$ substitution of $Mg^{2+} + Si^{4+} = Ti^{3+} + Al^{3+}$ (cpx or opx), there are:

$a = -0.89292$, $b = 3.012 \times 10^{-2}$, $c = -9.991 \times 10^{-4}$ for $Mg_{15}TiCa_{16}Si_{31}AlO_{96}$ (clinopyroxene) with Ti/(Ti+Si) = 1/32;

$a = -0.91643$, $b = 3.060 \times 10^{-2}$, $c = -1.015 \times 10^{-3}$ for $Mg_{31}TiSi_{31}AlO_{96}$ (orthopyroxene) with Ti/(Ti+Si) = 1/32.

For $Ti^{4+}$ substitution of $Si^{4+} = Ti^{4+}$ (opx), there are:

$a = -0.02689$, $b = 8.900 \times 10^{-4}$, $c = -3.100 \times 10^{-5}$ for $Mg_{32}Si_{31}TiO_{96}$ (orthopyroxene) with Ti/(Ti+Si) = 1/32;

$a = -0.04235$, $b = 1.170 \times 10^{-3}$, $c = -3.900 \times 10^{-5}$ for $Mg_{64}Si_{63}TiO_{192}$ (orthopyroxene) with Ti/(Ti+Si) = 1/64.

Overall, isotope fractionation factors of either $Ti^{3+}$ or $Ti^{4+}$ turn out to be identical between orthopyroxene and clinopyroxene[23]. For systems containing only $Ti^{4+}$, Ti-rich oxides (e.g., rutile, ilmenite, and magnetite) show $10^3 ln\alpha$ values lower by ~0.7–1.0‰ relative to those of orthopyroxene and clinopyroxene at 1000 K[23]. However, the crystallization of rutile, ilmenite, and magnetite usually requires $fO_2$ conditions exceeding typical $fO_2$ conditions in ureilites, diogenites, and shergottites or very evolved melt composition with MgO <5 wt.%. Therefore, we consider in this study mainly the Ti isotope fractionation factors (i.e., $10^3 ln\alpha$) of $Ti^{3+}$ and $Ti^{4+}$ in orthopyroxene and clinopyroxene, respectively, at 1473 *K*:

$$10^3 ln\alpha\left(Ti^{3+}{}_{opx/cpx} - Ti^{4+}{}_{opx/cpx}\right) = -0.450‰ \quad (6)$$

ii) Studies of Earth's mantle and mantle-derived rocks, which are characterized by $fO_2$ conditions with predominantly $Ti^{4+}$, show that at equilibrium there is negligible Ti isotope fractionation between orthopyroxene/clinopyroxene and basaltic silicate melts, that is:

$$10^3 ln\alpha\left(Ti^{4+}{}_{opx/cpx} - Ti^{4+}{}_{melt}\right) = +0.000‰ \quad (7)$$

While neither experimental nor theoretical constraint on $Ti^{3+}$ in silicate melt exists, we can assume for $Ti^{3+}$:

$$10^3 ln\alpha\left(Ti^{3+}{}_{opx/cpx} - Ti^{3+}{}_{melt}\right) = +0.000‰ \quad (8)$$

Afterwards, we can combine Eqs. 2 to 4 and 6 to 8 to calculate the equilibrium Ti isotope fractionation factor between mineral and melt at varying $fO_2$:

$$10^3 ln\alpha(mineral - melt) = \left[X^{Ti^{3+}}(opx/cpx) - X^{Ti^{3+}}(melt)\right] \times 10^3 ln\alpha\left(Ti^{3+}{}_{opx/cpx} - Ti^{4+}{}_{opx/cpx}\right) \quad (9)$$

The Ti isotopic effects of $Ti^{3+}$ and $Ti^{4+}$ during partial melting of a chondritic precursor can be further quantified via a Rayleigh process:

$$\Delta^{49}Ti_{melting\ residue-chondritic\ precursor} = -10^3 ln\alpha(mineral - melt) \times ln(f_{Ti}) \quad (10)$$

where $f_{Ti}$ represents the Ti fraction remaining in the melting residue after melt extraction, e.g., $f_{Ti} = 0.2$ adopted in Figs. 2C, 3, 5. The modeled $\delta^{49}Ti$ value of the melting residue should be:

$$\delta^{49}Ti_{melting\ residue} = \delta^{49}Ti_{chondrite} + \Delta^{49}Ti_{melting\ residue-chondritic\ precursor} \quad (11)$$

where the chondrite average has been adopted here, i.e., $\delta^{49}Ti = +0.053‰$[26]. Overall, integrating Eqs. 1 to 11 provides the modeling curves for Ti isotopic effects from $Ti^{3+}$ during melt extraction in Figs. 2C, 3, 5.

III. Key variables to the model

i) Equilibrium Ti isotope fractionation factors

We note that $10^3 ln\alpha(Ti^{3+}{}_{opx/cpx} - Ti^{4+}{}_{opx/cpx})$ and $10^3 ln\alpha(Ti^{4+}{}_{opx/cpx} - Ti^{4+}{}_{melt})$ can be estimated based on first-principles calculations and studies of Earth's mantle and mantle-derived rocks, respectively. In comparison, $10^3 ln\alpha(Ti^{3+}{}_{opx/cpx} - Ti^{3+}{}_{melt})$ is relatively uncertain. Nonetheless, choosing instead a $10^3 ln\alpha(Ti^{3+}{}_{opx/cpx} - Ti^{3+}{}_{melt})$ value of –0.050‰ in Eq. 8 would only lead to shifts of ≤0.011‰ in the predicted $\delta^{49}Ti$ values of the residual mantle after melt extraction at $f_{Ti}$ value of 0.2 and $fO_2$ conditions of ≥ ΔIW–3. Such insensitivity of the predicted Ti isotope fractionation in the residual mantle to the chosen $10^3 ln\alpha(Ti^{3+}{}_{opx/cpx} - Ti^{3+}{}_{melt})$ value arises from a fact that proportion of $Ti^{3+}$ remains low (≤14%) in basaltic silicate melts at $fO_2$ conditions of ≥ΔIW–3.

We also have to point out that the $10^3 ln\alpha(Ti^{3+}{}_{opx/cpx} - Ti^{4+}{}_{opx/cpx})$ value of –0.450‰ at 1473 K was chosen based on existing first-principles calculations on $Ti^{3+}$ substitution of $Mg^{2+} + Si^{4+} = Ti^{3+} + Al^{3+}$ for orthopyroxene or clinopyroxene[23], which is largely true for most planetary magma systems. This $Ti^{3+}$ substitution however can be suppressed in an Al-poor and Ti-rich system (e.g., the parent magmas of lunar mare basalts), which may lead to distinct Ti isotopic effects. For instance, petrological experiments using a mare basalt-like starting material (i.e., $SiO_2$ = 43.06 wt%, $TiO_2$ = 22.06 wt%, $Al_2O_3$ = 5.25 wt%, MgO = 22.47 wt%, and CaO = 8.09 wt%) provide slightly positive $10^3 ln\alpha$(mineral − melt) values of +0.050 ± 0.021‰ to +0.057 ± 0.037‰ at $fO_2$ conditions of ΔIW–1 to ΔIW + 0[41]. As such, more experimental or theoretical calibrations would be required if aiming to trace $fO_2$ conditions of the Moon with Ti isotopes.

ii) Remaining Ti fraction in melting residue ($f_{Ti}$)

Assuming a Rayleigh process for melt extraction, the magnitude of Ti isotope fractionation left in the residual mantle would be controlled by $10^3 ln\alpha$(mineral − melt) and $f_{Ti}$ (Eq. 10). For the chosen equilibrium Ti isotope fractionation factors of $Ti^{3+}$ and $Ti^{4+}$ in minerals and silicate melts (Eqs. 6 to 8), a $f_{Ti}$ value of 0.2 provides the modeling results that fit best with the $\delta^{49}Ti$ data from ureilites and diogenites (Fig. 3). Such a $f_{Ti}$ value is well consistent with a fractional melting process of a chondritic precursor with an average $D_{Ti}$ value of 0.15 and a partial melting degree of 0.2. For $f_{Ti}$ = 0.35, the Ti isotope fractionation in the residual mantle is predicted to be weaker (Fig. 2C), which cannot account for the lowest $\delta^{49}Ti$ values observed for ureilites (down to –0.105 ± 0.019‰) and diogenites (down to –0.039 ± 0.004‰).

iii) Chondrite $\delta^{49}Ti$ average

Recently, a Ti isotope method has been developed via Neoma MC-ICP-MS for concomitant determination of $\delta^{49}Ti$ and $\varepsilon^{50}Ti$ in meteorites at external reproducibilities of ±0.010‰ and ±0.15 epsilon, respectively[26]. Using this method, the $\delta^{49}Ti$ average of chondrites has been recommended to be +0.053 ± 0.005‰ (2se, $n$ = 22), including 22 chondrites for the average (i.e., 1 CI, 1 CV, 6 CM, 2 CO, 1 CH, 2 CK, 4 CR, 1 EH, 3 L, and 1 LL). However, a different $\delta^{49}Ti$ average (+0.023 ± 0.009‰, 2se, $n$ = 20) for chondrites was later proposed based on measurements of 10 ordinary chondrites by three laboratories[72]. According to Eq. 11, a decrease of 0.030‰ in the adopted chondrite $\delta^{49}Ti$ average can lead to an equivalent downward shift of the modeling curves in Figs. 2C, 3, 5. Afterwards, a higher $f_{Ti}$ value may be required to reduce the Ti isotope fractionation from melt extraction to account for the $\delta^{49}Ti$ data of ureilites, diogenites, and martian meteorites. Such a shift is much weaker if combining the two datasets for the estimate of chondrite $\delta^{49}Ti$ average, i.e., +0.044 ± 0.006‰ (2se, $n$ = 32).

We notice that for the same ordinary chondrite samples (e.g., Estacado and Richardton) in ref. 72, the $\delta^{49}Ti$ values obtained by the three included laboratories can differ by up to 0.068‰ (Supplementary Fig. S2), manifesting large analytical uncertainties associated with their published $\delta^{49}Ti$ dataset. In conjunction with the 2*sd* values of ±0.024‰ to ± 0.049‰ in $\delta^{49}Ti$ for their geostandards, the $\delta^{49}Ti$ data of ordinary chondrites from ref. 72 are three- to four-fold less precise compared to those reported in ref. 26 (Supplementary Fig. S2). Overall, the $\delta^{49}Ti$ average of +0.053 ± 0.005‰ from ref. 26 seems to be the best estimate for chondrites so far if taking into account the following additional lines of evidence:

a) The ~3.8 Ga Isua metabasalts in ref. 26 show a $\delta^{49}Ti$ average of +0.048 ± 0.005‰ (2se, $n$ = 5), and this average has been reproduced by ref. 73 (+0.046 ± 0.016‰, 2se, $n$ = 11). The studied ~3.8 Ga Isua metabasalts in ref. 26 have MgO ≥7.05 wt%, $FeO_T$ ≤13.21 wt%, and $TiO_2$ ≤1.518 wt%, which are unlikely to reach Fe-Ti oxide saturation under $fO_2$ conditions relevant to Earth's upper mantle (~ΔFMQ + 0)[74]. Also, the ~3.48 Ga Barberton komatiites and basaltic komatiites provide consistent $\delta^{49}Ti$ average values of +0.044 ± 0.009‰ (2se, $n$ = 4) and +0.048 ± 0.008‰ (2se, $n$ = 4). All these averages of Earth's early Archean mantle-derived rocks are well consistent with the $\delta^{49}Ti$ average of +0.053 ± 0.005‰ for bulk chondrites from ref. 26 or the $\delta^{49}Ti$ estimate of +0.044 ± 0.006‰ for bulk chondrites by combining the chondrite data from refs. 26, 72.

b) The oxidized ureilite sample EET 87517 in this study provides a $\delta^{49}Ti$ value of +0.052 ± 0.004‰, which, as modeled in Fig. 2C, likely records negligible isotopic effects from $Ti^{3+}$ and would most likely represent the $\delta^{49}Ti$ value of its chondritic precursor. Six of the studied diogenites from the Vesta asteroid show $\delta^{49}Ti$ values clustering around +0.053 ± 0.005‰. In addition, the studied shergottites define a positive correlation between $\delta^{49}Ti$ and $(La/Yb)_N$ and the enriched shergottites having $(La/Yb)_N$ values of ~0.75–1.15 show a $\delta^{49}Ti$ average of +0.043 ± 0.015‰ (2se, $n$ = 10). All these suggest that Mars and the parent bodies of ureilites and diogenites have bulk $\delta^{49}Ti$ values that are in line with the recommended $\delta^{49}Ti$ average for chondrites in ref. 26 (i.e., +0.053 ± 0.005‰).

iv) Influence of model variables on the constrained initial $fO_2$ of the martian mantle

Note that the depleted shergottites have been characterized by $\delta^{49}Ti$ values that are transitional between those of diogenites and ureilites. Accepting that the enrichments of the light Ti isotopes in diogenites, ureilites and depleted shergottites arise from the presence of $Ti^{3+}$ in the magma systems, the $fO_2$ conditions during early mantle differentiation of Mars at ~4.5 Ga would range between that of ureilites (~ΔIW–3.3 to ~ΔIW–1.5) and diogenites (~ΔIW–2 to ~ΔIW–0), irrespective of the above-mentioned model variables.

### Reporting summary

Further information on research design is available in the Nature Portfolio Reporting Summary linked to this article.

## Data availability

All research data are available in the Supplementary Information file and as well uploaded on the Figshare data repository (DOI: 10.6084/m9.figshare.29820956).

Received: 25 February 2025; Accepted: 11 August 2025;
Published online: 02 September 2025

## References

1. Hirschmann, M. M. Magma ocean influence on early atmosphere mass and composition. *Earth Planet. Sci. Lett.* **341**, 48–57 (2012).
2. Sossi, P. A. et al. Redox state of Earth's magma ocean and its Venus-like early atmosphere. *Sci. Adv.* **6**, eabd1387 (2020).
3. Gaillard, F. et al. Redox controls during magma ocean degassing. *Earth Planet. Sci. Lett.* **577**, 117255 (2022).
4. Deng, J. et al. A magma ocean origin to divergent redox evolutions of rocky planetary bodies and early atmospheres. *Nat. Commun.* **11**, 2007 (2020). p.
5. Armstrong, L. S. et al. Speciation and solubility of reduced C-O-H-N volatiles in mafic melt: Implications for volcanism, atmospheric evolution, and deep volatile cycles in the terrestrial planets. *Geochim. Cosmochim. Acta* **171**, 283–302 (2015).
6. Wood, B. J., Walter, M. J. & Wade, J. Accretion of the Earth and segregation of its core. *Nature* **441**, 825–833 (2006).
7. Righter, K., Drake, M. J. & Yaxley, G. Prediction of siderophile element metal-silicate partition coefficients to 20 GPa and 2800 degrees C: the effects of pressure, temperature, oxygen fugacity, and silicate and metallic melt compositions. *Phys. Earth Planet. Inter.* **100**, 115–134 (1997).
8. Herd, C. D. K. et al. Oxygen fugacity and geochemical variations in the martian basalts: Implications for martian basalt petrogenesis and the oxidation state of the upper mantle of Mars. *Geochim. Cosmochim. Acta* **66**, 2025–2036 (2002).
9. Herd, C. D. K., Papike, J. J. & Brearley, A. J. Oxygen fugacity of martian basalts from electron microprobe oxygen and TEM-EELS analyses of Fe-Ti oxides. *Am. Min.* **86**, 1015–1024 (2001).
10. Wadhwa, M. Redox state of Mars' upper mantle and crust from Eu anomalies in shergottite pyroxenes. *Science* **291**, 1527–1530 (2001).
11. Papike, J. J., Karner, J. M. & Shearer, C. K. Comparative planetary mineralogy: V/(Cr + Al) systematics in chromite as an indicator of relative oxygen fugacity. *Am. Min.* **89**, 1557–1560 (2004).
12. Karner, J. M. et al. Valence state partitioning of Cr and V between pyroxene-melt: Estimates of oxygen fugacity for martian basalt QUE 94201. *Am. Min.* **92**, 1238–1241 (2007).
13. Papike, J. J. et al. Chromium, vanadium, and titanium valence systematics in Solar System pyroxene as a recorder of oxygen fugacity, planetary provenance, and processes. *Am. Min.* **101**, 907–918 (2016).
14. Righter, K. et al. Redox variations in the inner solar system with new constraints from vanadium XANES in spinels. *Am. Min.* **101**, 1928–1942 (2016).
15. Herd, C. D. K. The oxygen fugacity of olivine-phyric martian basalts and the components within the mantle and crust of Mars. *Meteorit. Planet. Sci.* **38**, 1793–1805 (2003).
16. McCanta, M. C., Rutherford, M. J. & Jones, J. H. An experimental study of rare earth element partitioning between a shergottite melt and pigeonite: implications for the oxygen fugacity of the Martian interior. *Geochim. Cosmochim. Acta* **68**, 1943–1952 (2004).
17. Righter, K. et al. Oxygen fugacity in the Martian mantle controlled by carbon: new constraints from the nakhlite MIL 03346. *Meteorit. Planet. Sci.* **43**, 1709–1723 (2008).
18. Nicklas, R. W. et al. Uniform oxygen fugacity of shergottite mantle sources and an oxidized Martian lithosphere. *Earth Planet. Sci. Lett.* **564**, 116876 (2021).
19. Chen, J.-F. et al. The oxygen fugacity of intermediate shergottite NWA 11043: implications for Martian mantle evolution. *Geochim. Cosmochim. Acta* **375**, 90–105 (2024).
20. Day, J. M. D. et al. Martian magmatism from plume metasomatized mantle. *Nat. Commun.* **9**, 4799 (2018).
21. Wadhwa, M. Redox conditions on small bodies, the Moon and Mars. *Oxyg. Sol. Syst.* **68**, 493–510 (2008).
22. Mallmann, G. & O'Neill, H. S. C. The crystal/melt partitioning of V during mantle melting as a function of oxygen fugacity compared with some other elements (Al, P, Ca, Sc, Ti, Cr, Fe, Ga, Y, Zr and Nb). *J. Petrol.* **50**, 1765–1794 (2009).
23. Wang, W. Z. et al. Equilibrium inter-mineral titanium isotope fractionation: Implication for high-temperature titanium isotope geochemistry. *Geochim. Cosmochim. Acta* **269**, 540–553 (2020). p.
24. Millet, M. A. et al. Titanium stable isotope investigation of magmatic processes on the Earth and Moon. *Earth Planet. Sci. Lett.* **449**, 197–205 (2016).
25. Deng, Z. et al. Lack of resolvable titanium stable isotopic variations in bulk chondrites. *Geochim. Cosmochim. Acta* **239**, 409–419 (2018).
26. Deng, Z. et al. Earth's evolving geodynamic regime recorded by titanium isotopes. *Nature* **621**, 100–104 (2023).
27. Goodrich, C. A. et al. Metallic phases and siderophile elements in main group ureilites: Implications for ureilite petrogenesis. *Geochim. Cosmochim. Acta* **112**, 340–373 (2013).
28. Goodrich, C. A., Van Orman, J. A. & Wilson, L. Fractional melting and smelting on the ureilite parent body. *Geochim. Cosmochim. Acta* **71**, 2876–2895 (2007).
29. Goodrich, C. A. Ureilites: a critical review. *Meteoritics* **27**, 327–352 (1992).
30. Warren, P. H. & Kallemeyn, G. W. Explosive volcanism and the graphite oxygen fugacity buffer on the parent asteroid(s) of the ureilite meteorites. *Icarus* **100**, 110–126 (1992).
31. Barrat, J. A. et al. Partial melting of a C-rich asteroid: lithophile trace elements in ureilites. *Geochim. Cosmochim. Acta* **194**, 163–178 (2016).
32. Fowler, G. W. et al. Diogenites as asteroidal cumulates - Insights from ortho-pyroxene major and minor element chemistry. *Geochim. Cosmochim. Acta* **58**, 3921–3929 (1994).
33. Yamaguchi, A. et al. Posteucritic magmatism on Vesta: Evidence from the petrology and thermal history of diogenites. *J. Geophys. Res. Planets* **116**, E08009 (2011).
34. Collinet, M. & Grove, T. L. Widespread production of silica- and alkali -rich melts at the onset of planetesimal melting. *Geochim. Cosmochim. Acta* **277**, 334–357 (2020).
35. Burns, R. G. & Martinez, S. L. Mössbauer spectra of olivine-rich achhondrites: evidence from preterrestrial redox reactions. *Proc. Lunar Planet. Sci.* **21**, 331–340 (1991).
36. Deng, Z., et al. Early oxidation of the martian crust triggered by impacts. *Sci. Adv.* **6**, eabc4941 (2020).
37. Deng, Z. et al. Titanium isotopes as a tracer for the plume or island arc affinity of felsic rocks. *Proc. Natl. Acad. Sci. USA* **116**, 1132–1135 (2019).
38. Johnson, A. C. et al. Titanium isotopic fractionation in Kilauea Iki lava lake driven by oxide crystallization. *Geochim. Cosmochim. Acta* **264**, 180–190 (2019).
39. Hoare, L. et al. Melt chemistry and redox conditions control titanium isotope fractionation during magmatic differentiation. *Geochim. Cosmochim. Acta* **282**, 38–54 (2020).
40. Zhao, X. M. et al. Titanium isotopic fractionation during magmatic differentiation. *Contrib. Mineral. Petrol.* **175**, 67 (2020).
41. Rzehak, L. J. A. et al. The redox dependence of titanium isotope fractionation in synthetic Ti-rich lunar melts. *Contrib. Mineral. Petrol.* **176**, 3 (2021).

42. Borisov, A. A. The $Ti^{3+}/Ti^{4+}$ ratio of magmatic melts: application to the problem of the reduction of lunar basalts. *Petrology* **20**, 391–398 (2012).
43. Guilherme, M., Antony, D. B. & Raul O. C. F. in *Magma Redox Geochemistry* (eds Neuville, D. R. & Moretti, R.) (Wiley, 2021).
44. Berry, A. J. et al. The oxidation state of titanium in silicate melts. *Geochim. Cosmochim. Acta* **366**, 210–220 (2024).
45. Trinquier, A. et al. Origin of nucleosynthetic isotope heterogeneity in the solar protoplanetary disk. *Science* **324**, 374–376 (2009).
46. Sutton, S. R., Goodrich, C. A. & Wirick, S. Titanium, vanadium and chromium valences in silicates of ungrouped achondrite NWA 7325 and ureilite Y-791538 record highly-reduced origins. *Geochim Cosmochim. Acta* **204**, 313–330 (2017).
47. Borg, L. E. et al. Constraints on Martian differentiation processes from Rb-Sr and Sm-Nd isotopic analyses of the basaltic shergottite QUE 94201. *Geochim. Cosmochim. Acta* **61**, 4915–4931 (1997).
48. Borg, L. E. et al. The age of Dar al Gani 476 and the differentiation history of the martian meteorites inferred from their radiogenic isotopic systematics. *Geochim. Cosmochim. Acta* **67**, 3519–3536 (2003).
49. Blichert-Toft, J. et al. The Lu-Hf isotope geochemistry of shergottites and the evolution of the Martian mantle-crust system. *Earth Planet. Sci. Lett.* **173**, 25–39 (1999).
50. Debaille, V. et al. Coupled $^{142}$Nd-$^{143}$Nd evidence for a protracted magma ocean in Mars. *Nature* **450**, 525–528 (2007).
51. Armytage, R. M. G. et al. A complex history of silicate differentiation of Mars from Nd and Hf isotopes in crustal breccia NWA 7034. *Earth Planet. Sci. Lett.* **502**, 274–283 (2018).
52. Borg, L. E., Brennecka, G. A. & Symes, S. J. K. Accretion timescale and impact history of Mars deduced from the isotopic systematics of martian meteorites. *Geochim. Cosmochim. Acta* **175**, 150–167 (2016).
53. Righter, K. & Drake, M. J. Core formation in Earth's Moon, Mars, and Vesta. *Icarus* **124**, 513–529 (1996).
54. Khan, A. et al. Geophysical and cosmochemical evidence for a volatile-rich Mars. *Earth Planet. Sci. Lett.* **578**, 117330 (2022).
55. Bouvier, L. C. et al. Evidence for extremely rapid magma ocean crystallization and crust formation on Mars. *Nature* **558**, 586–589 (2018).
56. Costa, M. M. et al. The internal structure and geodynamics of Mars inferred from a 4.2-Gyr zircon record. *Proc. Natl. Acad. Sci. USA* **117**, 30973–30979 (2020).
57. Pan, L., Deng, Z. B. & Bizzarro, M. Impact induced oxidation and its implications for early Mars climate. *Geophys. Res. Lett.* **50**, e2023GL102724 (2023).
58. Frost, D. J. & McCammon, C. A. The redox state of Earth's mantle. *Annu. Rev. Earth Planet. Sci.* **36**, 389–420 (2008).
59. Trail, D., Watson, E. B. & Tailby, N. D. The oxidation state of Hadean magmas and implications for early Earth's atmosphere. *Nature* **480**, 79–82 (2011).
60. Frost, D. J. et al. Experimental evidence for the existence of iron-rich metal in the Earth's lower mantle. *Nature* **428**, 409–412 (2004).
61. Frost, D. J. et al. The redox state of the mantle during and just after core formation. *Philos. Trans. R. Soc. A Math. Phys. Eng. Sci.* **366**, 4315–4337 (2008).
62. Armstrong, K. et al. Deep magma ocean formation set the oxidation state of Earth's mantle. *Science* **365**, 903–906 (2019).
63. Zhang, H. L., et al. Ferric iron stabilization at deep magma ocean conditions. *Sci. Adv.* **10**, eadp1752 (2024).
64. Zahnle, K. et al. Photochemical instability of the ancient Martian atmosphere. *J. Geophys. Res.Planets* **113**, E11004 (2008).
65. Liggins, P., Shorttle, O. & Rimmer, P. B. Can volcanism build hydrogen-rich early atmospheres?. *Earth Planet. Sci. Lett.* **550**, 116546 (2020).
66. Villanueva, G. L. et al. Strong water isotopic anomalies in the martian atmosphere: Probing current and ancient reservoirs. *Science* **348**, 218–221 (2015).
67. Urey, H. C. On the early chemical history of the Earth and the origin of life. *Proc. Natl. Acad. Sci. USA* **38**, 351–363 (1952).
68. Kasting, J. F. Earths early atmosphere. *Science* **259**, 920–926 (1993).
69. Ramirez, R. M. et al. Warming early Mars with $CO_2$ and $H_2$. *Nat. Geosci.* **7**, 59–63 (2014).
70. Wordsworth, R. et al. Transient reducing greenhouse warming on early Mars. *Geophys. Res. Lett.* **44**, 665–671 (2017).
71. Zhang, J. J. et al. A new method for MC-ICPMS measurement of titanium isotopic composition: identification of correlated isotope anomalies in meteorites. *J. Anal. At. Spectrom.* **26**, 2197–2205 (2011).
72. Anguelova, M. et al. Constraining the mass-dependent Ti isotope composition of the chondritic reservoir – an inter-laboratory comparison study. *Geochim. Cosmochim. Acta* **372**, 171–180 (2024).
73. Hoare, L. et al. Titanium isotope constraints on the mafic sources and geodynamic origins of Archean crust. *Geochem. Perspect. Lett.* **28**, 37–42 (2023).
74. Toplis, M. J. & Carroll, M. R. An experimental-study of the influence of oxygen fugacity on Fe-Ti oxide stability, phase-relations, and mineral-melt equilibria in ferro-basaltic systems. *J. Petrol.* **36**, 1137–1170 (1995).
75. Mcdonough, W. F. & Sun, S. S. The composition of the Earth. *Chem. Geol.* **120**, 223–253 (1995).
76. Brennan, M. C., Fischer, R. A. & Irving, J. C. E. Core formation and geophysical properties of Mars. *Earth Planet. Sci. Lett.* **530**, 115923 (2020).


## Acknowledgements

We thank C. Cloquet for sharing the OL-Ti standard. This research is funded by the National Natural Science Foundation of China (42373040 to Z.D.), the National Key Research and Development Program of China (2024YFF0809800 to L.P.), the Carlsberg Foundation (CF18-1105 to M.B. and CF20_0209 to M.S.), the Villum Fonden (no. 00025333 to M.S.), and the European Research Council (ERC Advanced Grant agreement no. 833275-DEEPTIME to M.B.).

## Author contributions

Z.D. conceived the idea and designed the project; Z.D., M.S. and L.P. contributed the methodology; Z.D., M.S. and M.B. selected the samples for study; Z.D. and K.N. carried out the research and analyzed the data; Z.D. interpreted the data; Z.D. and L.P. wrote the manuscript with inputs from K.N., M.S., W.W. and M.B.

## Competing interests

The authors declare no competing interests.

## Additional information

**Supplementary information** The online version contains supplementary material available at https://doi.org/10.1038/s43247-025-02692-5.

**Correspondence** and requests for materials should be addressed to Zhengbin Deng.

**Peer review information** *Communications Earth and Environment* thanks Paolo Sossi and the other, anonymous, reviewer(s) for their contribution to the peer review of this work. Peer review was single-anonymous OR Peer review was double-anonymous. Primary Handling Editors: Claire Nichols, Somaparna Ghosh, Carolina Ortiz Guerrero [A peer review file is available].